Ore Geology Reviews 117 (2020) 103308

Contents lists available at ScienceDirect

Ore Geology Reviews

journal homepage: www.elsevier.com/locate/oregeorev

Cobalt enrichment in a paleo-karstic bauxite deposit at Yunfeng, Guizhou Province, SW China

Yongzhen Long[a,b,*], Anhuai Lu[a,b], Xiangping Gu[a,b], Guoxiang Chi[c,*], Lin Ye[d], Zhongguo Jin[e], Dongliang Zhang[a,b]

[a] Key Laboratory of Metallogenic Prediction of Nonferrous Metals and Geological Environment Monitoring, Ministry of Education, Central South University, Changsha 410083, China
[b] School of Geosciences and Info-Physics, Central South University, Changsha 410083, China
[c] Department of Geology, University of Regina, Saskatchewan S4S 0A2, Canada
[d] State Key Laboratory of Ore Deposit Geochemistry, Institute of Geochemistry, Chinese Academy of Sciences, Guiyang 550002, China
[e] Non-Ferrous Metals and Nuclear Industry Geological Exploration Bureau of Guizhou, Guiyang 550005, China

ARTICLE INFO

Keywords:
Cobalt
Enrichment
Sulfide
Sulfoarsenide
Bauxite deposit

ABSTRACT

Cobalt can be enriched in a variety of different geologic settings, while it is mainly produced as a by-product of sediment-hosted stratiform Cu deposits and magmatic Ni-Cu deposits associated with mafic and ultramafic rocks. In this study, we report elevated Co concentrations in a paleo-karstic bauxite deposit at Yunfeng, Guizhou Province. Whole-rock chemical analyses indicate that Co is concentrated in carbonaceous ferruginous clay layers (167–962 ppm, average 383 ppm, n = 5) and siderite layers (47–439 ppm, average 213 ppm, n = 7) within the bauxite deposit. The positive correlation between Co and S, together with petrographic and EPMA analyses, suggests that Co occurs primarily as Co-rich/bearing sulfides/sulfoarsenides rather than cobaltiferous oxides/hydroxides as in most lateritic Ni-Co deposits. Many of the Co concentrations measured in this study are higher than the minimum grade (300 ppm) or cut-off grade (200 ppm) for economic exploitation of Co from sulfides or arsenides. Basing on these results, we put forward the scientific significance of Co enrichment in paleo-karstic environments and the potential importance of Co resources (as by-products of aluminum production) in bauxite deposits.

1. Introduction

Cobalt (Co) is a strategic and critical metal, classified as an essential element for technological development by the European Union (Pazik et al., 2016). It is a compatible siderophile and chalcophile element, widely dispersed in the upper continental crust with an average abundance of only 17 ppm (Taylor and McLennan, 1985). Geological processes, such as magmatic differentiation, chemical weathering, and hydrothermal activity, are required to concentrate the metal into potentially exploitable deposits.

Cobalt is commonly found in sulfide/sulfoarsenide minerals associated with copper, nickel and iron (Hughes et al., 2016; Saintilan et al., 2017). Most of metallic Co is obtained as a by-product from (i) stratabound Cu-Co deposits hosted by sedimentary rocks (Grorud, 1997; Cailteux et al., 2005; Li et al., 2008; Saintilan et al., 2017); (ii) primary magmatic Ni-Cu-(Co-PGE) sulfide deposits (Naldrett et al., 2000; Hughes et al., 2016); (iii) hydrothermal and volcanogenic polymetallic deposits (Gervill et al., 1997; Wagner and Lorenz, 2002; Nimis et al., 2014); (iv) lateritic Ni-Co deposits (formed from weathering of ultramafic rocks, most notably in New Caledonia, Congo, Cuba, and Australia; Decrée et al., 2015; Muchez and Corbella, 2012; Yongue-Fouateu, et al., 2006; Pazik et al., 2016; Ugwu and Sherman, 2017; Gigler and Kinnaird, 2017); and (v) various hydrothermal polymetallic deposits, including the “Five-Element” deposits, skarn iron deposits, and other hydrothermal deposits of different origins (Kissin, 1992; Lefebure, 1996; Gervill et al., 1997; Wagner and Lorenz, 2002; Li et al., 2008; Desouky et al., 2010; Fay and Barton, 2012; Nimis et al., 2014; Naumov et al., 2017; Zou et al., 2018). Cobalt is also enriched within unconformity-related uranium deposits (Sibbald, 1985), sandstone-hosted uranium deposits (Ingham et al., 2014; Bonnetti et al., 2015), as well as in some black shales (Large et al., 1999; Gregory et al., 2015).

Paleo-karstic bauxite deposits, the main source of aluminum metal

* Corresponding authors.
E-mail addresses: longyongzhen@csu.edu.cn (Y. Long), guoxiang.chi@uregina.ca (G. Chi).

https://doi.org/10.1016/j.oregeorev.2019.103308
Received 25 September 2019; Received in revised form 14 December 2019; Accepted 31 December 2019
Available online 03 January 2020

in China, form as a result of accumulation of weathering products in paleo-karstic depressions (Bárdossy and Aleva, 1990; Bogatyrev et al., 2009). Elevated Co concentrations above the upper crustal value (17 ppm; Taylor and McLennan, 1985) have been reported in some paleo-karstic bauxite deposits, such as, up to 404 ppm (average 60.2 ppm, n = 11) in the Wachangping bauxite deposit, northern Guizhou, China (Huang et al., 2014); up to 349 ppm (median = 36.9, min = 5.3, std = 40.7, n = 57) in the bauxite deposits in central-southern Italy (Mongelli et al., 2017); and up to 208.7 ppm (average 48.2 ppm, n = 20) in the Zagrad bauxite deposit, Montenegro (Radusinović et al., 2017). However, it remains poorly understood how Co is distributed and in what form it occurs in the bauxite deposits, which seriously restricts further evaluation of cobalt as a by-product of aluminum production.

This study deals with the concentrations, occurrences, and distribution of Co in rocks from the Yunfeng bauxite deposit, based on field observations, along with optical microscopy, electron probe microanalysis (EPMA), atomic absorption spectrograph (AAS), X-ray fluorescence (XRF) and inductively coupled plasma–mass spectrometry (ICP-MS) analyses. The study results may provide theoretical support for exploitation of cobalt as a by-product of aluminum production processes, which may make paleo-karstic bauxite deposits a potential cobalt resource.

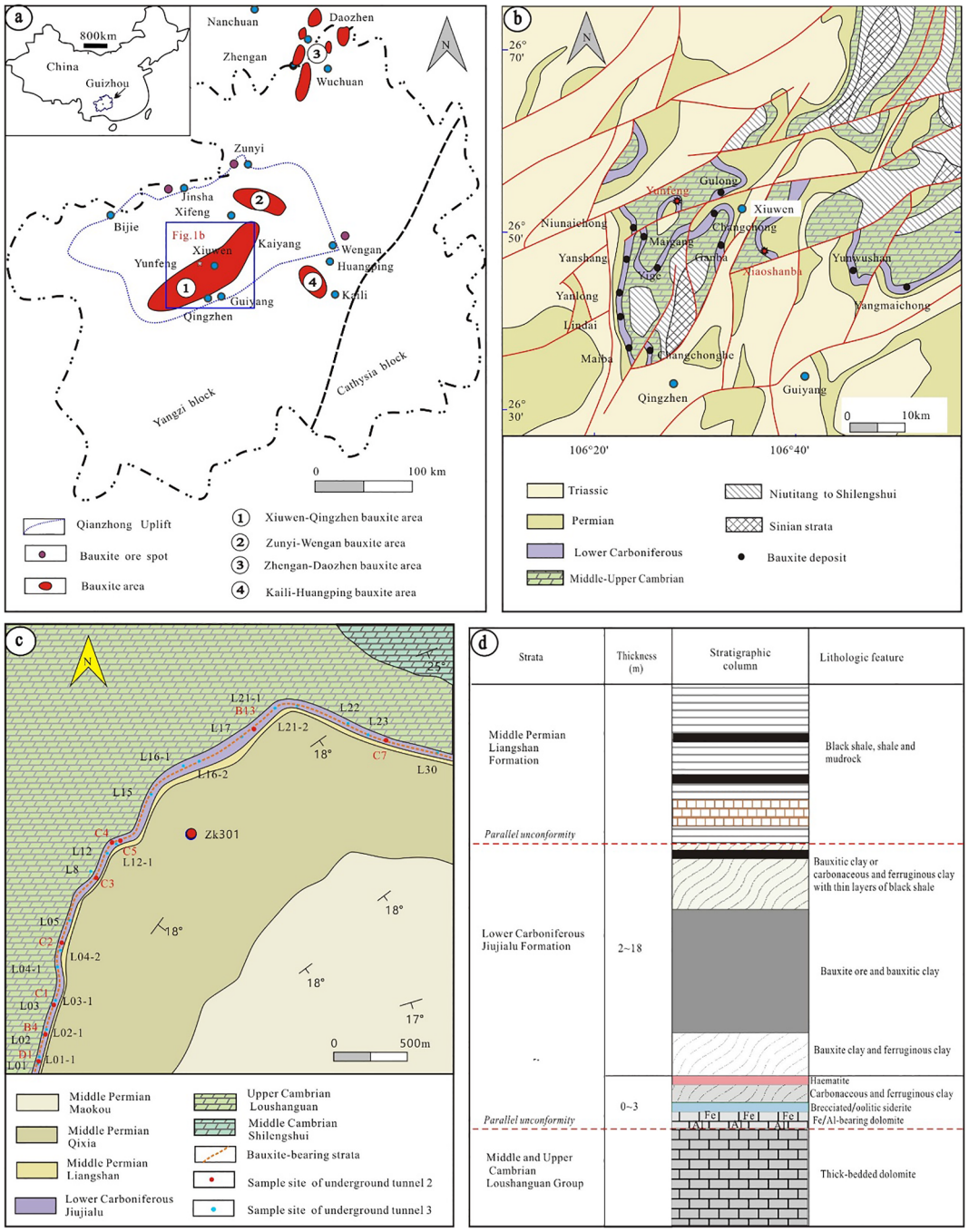

Fig. 1. (a) Sketch map showing the distribution of bauxite areas in Guizhou Province in South China; (b) Sketch geological map of the Xiuwen-Qingzhen bauxite area (modified from Long et al., 2017); (c) Geological map of underground tunnels 2 and 3 of the Yunfeng bauxite deposit showing the locations of samples examined in this study (modified from Yunfeng Mining Company, unpublished data, 2013 and 2017); (d) Lithostratigraphic column for the Xiuwen-Qingzhen bauxite area.

2. Geological setting and mineralization characteristics

The Yunfeng bauxite deposit is one of a number of paleo-karstic bauxite deposits in the Xiuwen-Qingzhen bauxite district in central Guizhou Province, southwestern China (Fig. 1a, b). This area is located in the Qianzhong Uplift within the Yangtze Block, where the exposed strata range in age from Late Sinian (Neoproterozoic) to Early Triassic, with a major hiatus between Upper Cambrian and Lower Carboniferous strata (Guizhou Bureau of Geology and Mineral Resources, 1987; Zhang et al., 2013; Ling et al., 2015; Long et al., 2017,2018). The bauxite mineralization occurs within the Lower Carboniferous Jiujialu Formation overlying unconformably the Upper Cambrian Loushanguan Group (Fig. 1b, c, d). The strata underlying the Loushanguan Group include, from upper to lower, Middle-Upper Cambrian Shilengshui and Gaotai formations, Lower Cambrian Qingxudong, Jindingshan, Mingxinsi and Niutitang formations, and Sinian Dengying Formation, whereas the strata above the Jiujialu Formation consist of, from lower to upper, Lower Carboniferous Baizuo Formation (partly equivalent to Jiujialu Formation), Permian Liangshan, Qixia and Maokou formations, and Lower Triassic Daye Formation (Fig. 1b, c). The bauxite-bearing Jiujialu Formation is sandwiched between dolomite of the Upper Cambrian Loushanguan Group and shale, mudrock and sandstone of the Permian Liangshan Formation. The Jiujialu Formation consists of mudrocks transitional to bauxite-rich clay units and bauxite orebodies, and the stratigraphy-equivalent Baizuo Formation is comprised of argillaceous dolomite (Guizhou Bureau of Geology and Mineral Resources, 1987; Ye et al., 2008; Long et al., 2017).

In the Yunfeng bauxite deposit, the Jiujialu Formation consists of eight layers (Fig. 1d) including, from bottom to top, (i) aluminous dolomite layer, (ii) ferruginous dolomite layer, (iii) siderite layer, (iv) carbonaceous ferruginous clay layer, (v) hematite layer, (vi) bauxitic and ferruginous clay layer, (vii) bauxite ore and bauxitic clay layer, and (viii) bauxitic and/or carbonaceous ferruginous clay layer with thin layers of black shale. The total thickness of layers (i)–(v) ranges from 0 to 3 m, and that of layers (vi)–(viii) ranges from 2 to 18 m (Fig. 1d). The bauxite ore and bauxitic clay layer is gradational to carbonaceous ferruginous clay above (Fig. 2a) and ferruginous clay below (Fig. 2b).

The bauxite ores are composed of diaspore, boehmite and clay minerals, with variable amounts of Fe-oxides/hydroxides and other minerals, whereas the bauxitic clays are dominated by clay minerals, with lesser amounts of boehmite and diaspore (Ling et al., 2015; Long et al., 2017,2018). The dolomite layer at the bottom of the Jiujialu Formation (Fig. 1d) is composed of massive dolomite (Fig. 2c), with variable amounts of clay minerals and Fe-oxides/hydroxides, and the overlying siderite layer is made up of siderite, with oolitic (Fig. 2d) or brecciated (Fig. 2e) structure, and contains variable amounts of clay minerals, Fe-, Al- and Mn-oxides/hydroxides and carbonaceous matter. The carbonaceous ferruginous clay layer, black gray to black in color (Fig. 2a), consists of clay minerals and carbonaceous materials. The ferruginous clay layer, grey brown (Fig. 2b) to reddish brown in color, comprises clay minerals and variable amounts of Fe-oxides/hydroxides.

3. Samples and analytical methods

Thirty-one (31) samples were collected from the Yunfeng deposit (one from an outcrop and 30 from underground tunnels; see Fig. 1c for locations) for mineralogical and geochemical studies. Polished thin sections made from these samples were studied for petrography and EPMA analysis. Whole-rock powders (crushed to 200 mesh) were analyzed with X-ray fluorescence (XRF), wet chemistry method, inductively coupled plasma–mass spectrometry (ICP-MS), atomic absorption spectrograph (AAS), and LECO. The EPMA, XRF and ICP-MS analyses were conducted at the School of Geosciences and Info-Physics, Central South University. The AAS, wet chemistry and LECO analyses were performed at the Analytical and Detection Centre of the Changsha Research Institute of Mining and Metallurgy.

The EPMA analysis of mineral composition was performed using a Shimadzu EPMA-1720H instrument equipped with a wavelength dispersive spectrometer (WDS) and an EDAX Genesis energy dispersive spectrometer (EDS). Analytical errors are 1% for major elements and 3% for minor elements, and the detection limit is 0.01%. Back scattered electron images were obtained at an accelerating voltage of 12 kV and a beam current of ~10 μA.

The major elements of powdered samples were analyzed with XRF

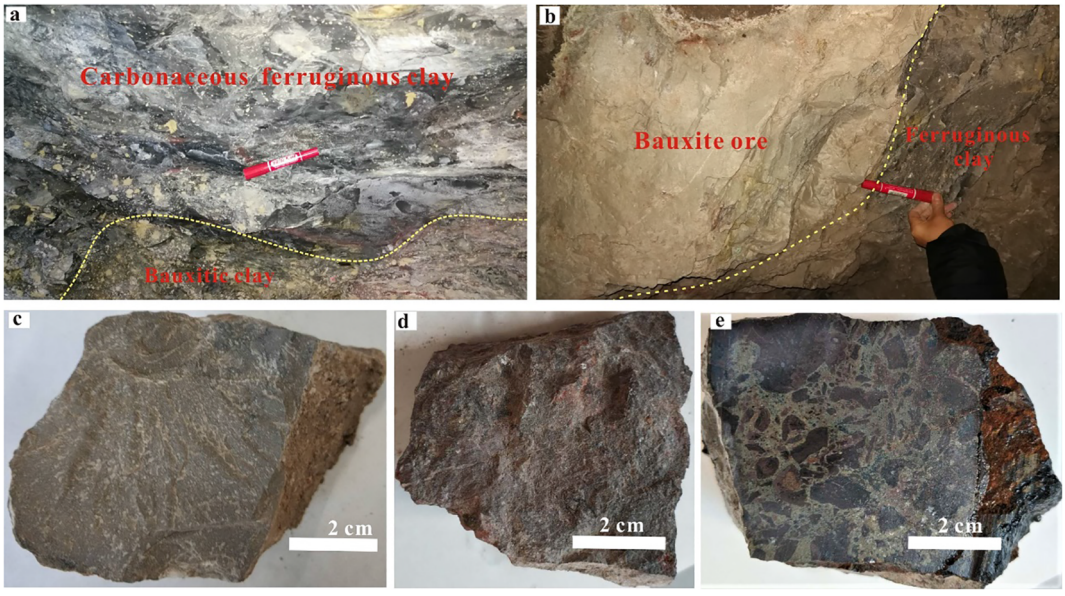

Fig. 2. Photos of representative samples/profiles from the Yunfeng bauxite deposit. (a) A profile showing carbonaceous-bearing ferruginous clay and bauxitic clay; (b) A profile showing ferruginous clay and bauxite ore; (c) Ferruginous dolomite; (d) Oolitic siderite; (e) Brecciated siderite layer.

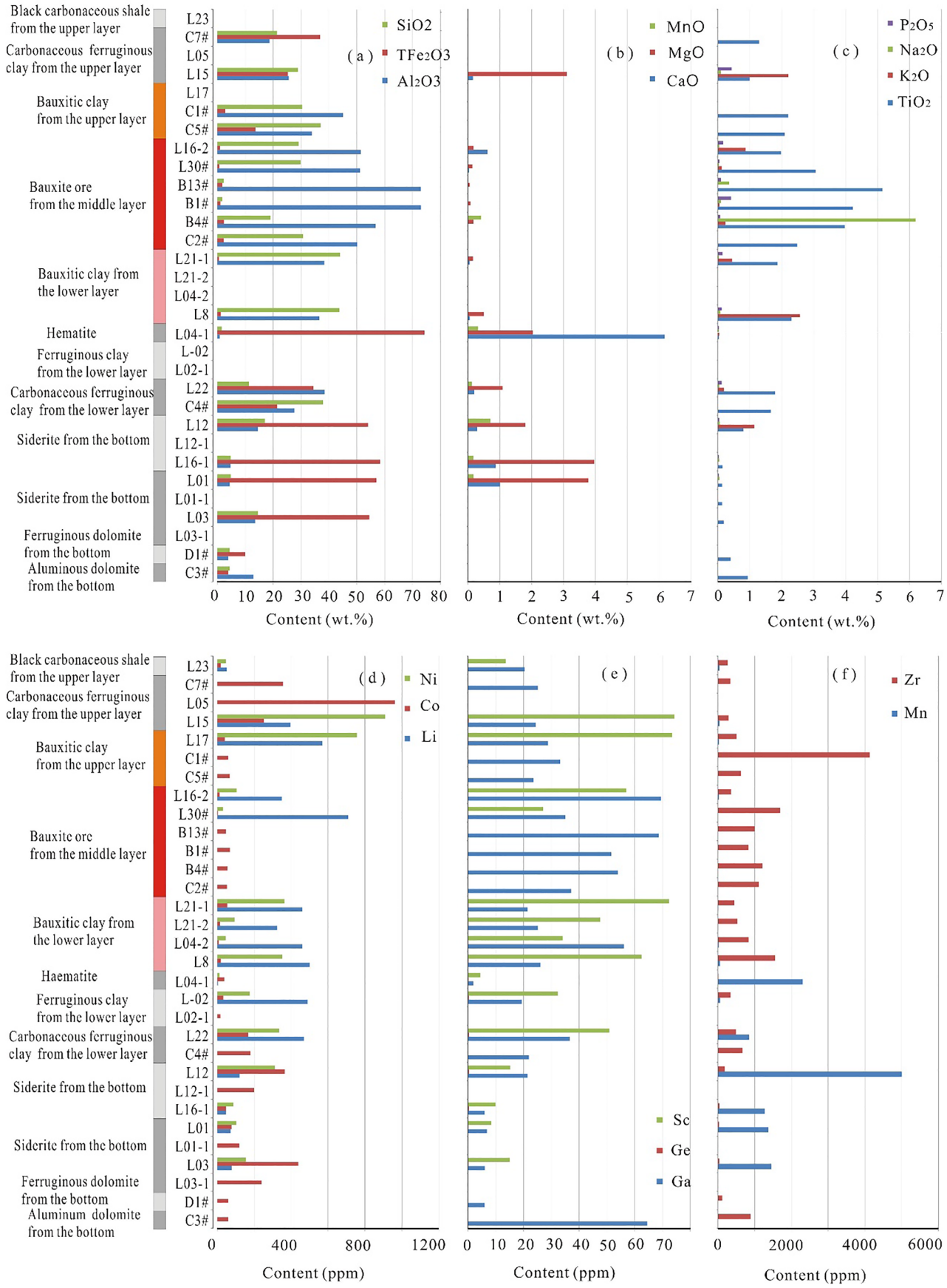

Fig. 3. Profiles of various elements across different layers in the Yunfeng bauxite deposit. (a) SiO_2, TFe_2O_3 and Al_2O_3; (b) MnO, MgO and CaO; (c) P_2O_5, Na_2O, K_2O and TiO_2; (d) Ni, Co and Li; (e) Sc, Ge and Ga; and (f) Zr and Mn.

Table 1
Correlation coefficients between Co and some major and trace elements in samples collected from the Yunfeng deposit, central Guizhou Province.*

Al_2O_3	TFe_2O_3	SiO_2	TiO_2	MgO	K_2O	P_2O_5	Na_2O	Li	S	Cr	Cu
−0.36	0.38	−0.03	−0.37	0.34	0.34	0.21	−0.11	−0.34	0.92	−0.30	0.32
Ni	Zn	Bi	Be	Ga	Sb	Th	U	V	Y	Ag	Ba
0.30	0.00	−0.34	−0.19	−0.32	0.00	−0.34	−0.24	0.27	0.38	0.07	0.16
Be	Ca	Cd	Cr	Cs	Hf	Ga	Ge	As	Mn	Mo	Nb
−0.21	−0.02	0.17	−0.26	−0.08	−0.26	−0.29	0.53	0.28	0.59	−0.15	−0.34
Se	Sc	Sn	Sr	Ta	Tl	W	Zr	Pb	LREE	HREE	
0.41	−0.15	−0.33	−0.02	−0.34	−0.03	−0.35	−0.27	−0.34	−0.22	0.29	

* Calculated from data in Supplementary Table 1.

and a wet chemistry method. The XRF analyses were performed using a Rigaku Primus II instrument. About 0.7 g of sample powder was mixed with 7 g composite flux (Li_2B4O7: $LiBO_2$: LiF = 4.5: 1: 0.4) in a platinum crucible and heated to 1150 °C in a melting chamber. Once the samples had liquefied, the heating was ceased, and the samples were left to cool and solidify prior to the XRF analysis. The total Fe content is given as Fe_2O_3. Loss on ignition (LOI) was measured by weighing the samples before and after 2 h of heating at 850 °C. The analytical precision is generally better than 5%. The quality of the wet chemistry analyses was controlled by duplicated samples and international standard samples (GBW07179, GBW07405), which yielded a precision better than 5%.

The trace elements of powdered samples were analyzed with ICP-MS and AAS. The ICP-MS analyses were conducted using an Agilent Technologies 7700x quadrupole instrument following the procedure described in Qi et al. (2000). Forty (40) mg of each sample was dissolved in a high-pressure Teflon beaker for 24 h at 190 °C using a HF + HNO_3 mixture. Rh was used as an internal standard to monitor signal drift during ICP-MS analysis, and international standards (AMH-1, OU-6, and GBPG-1) were used for calibration. The precision was within 4% for most rare earth elements and 6% for other trace elements. The AAS analyses were conducted with a PE PinAAcle 900 T instrument, following the analytical procedures described in GB/T 17141-1997. Five hundred (5 0 0) mg of powdered samples were dissolved in a high-pressure Teflon beaker for 24 h at 190 °C using a HF + HNO_3 + $HClO_4$ mixture. The analytical precision was within 3%.

Total sulfur (TS) contents were analyzed using a LECO SC632 elemental analyzer. About 100 mg of the powdered sample, after acidification using H_3PO_4 (10%) to remove carbonates, was placed in a porcelain crucible and combusted in a pure oxygen atmosphere at 1350℃. Released sulfur dioxide was quantified by an IR detector, yielding precision better than 7%.

4. Results

4.1. Whole-rock geochemistry

The results of major, trace and rare earth elements analyses of 31 representative rock and ore samples collected from the Yunfeng bauxite deposit are listed in Supplementary Table 1.

The geochemical data show that the main compositions of the siderite samples (n = 4) are Fe_2O_3 (54.02–58.41 wt%), SiO_2 (4.81–17.06 wt%), Al_2O_3 (4.45–1.59 wt%), TiO_2 (1.92–5.30 wt%) and MgO (1.80–3.96 wt%), followed by small amounts of MnO (0.17–0.70 wt%) and P_2O_5 (0.10–1.15 wt%) (Fig. 3; Supplementary Table 1). The hematite sample (n = 1) has the highest Fe_2O_3 (74.23 wt %). The samples of ferruginous clays and carbonaceous ferruginous clay (n = 7) contain high concentrations of As (386 ppm), Cu (2630 ppm), Ni (909 ppm), V (1280 ppm) and Y (895 ppm) (Fig. 3; Supplementary Table 1). The highest Zn (3700 ppm) and Zr (4300 ppm) are found in bauxitic clays (n = 4, both from the upper layer and lower layer), and the highest Al_2O_3, TiO_2, Li and Ga occur in the bauxite ores (n = 6) (Fig. 3; Supplementary Table 1).

Cobalt (Co) ranges from 47.4 to 439 (average = 212.8; median = 200) ppm for the siderite samples (n = 7); 167 to 962 (average = 383; median = 253) ppm for the carbonaceous ferruginous clay samples (n = 5) from both the upper and lower layer; 8.5 to 68 (average = 37.6; median = 40.8) ppm for the bauxitic clays (n = 7); and 4.0 to 69 (average = 40.2; median = 50) ppm for the bauxite ores (n = 6) (Supplementary Table 1, Fig. 3d).

Correlation analysis (Table 1; Fig. 4-1 and Fig. 4-2) reveals that Co has a strong positive correlation with S (R = 0.92) and moderate to weak positive correlation with TFe_2O_3 (R = 0.38); Mn (R = 0.59), MgO (R = 0.34), K_2O (R = 0.32), Ge (R = 0.59), Ni (R = 0.30), Se (R = 0.41), and Cu (R = 0.32) (Table 1; Fig. 4-1 and Fig. 4-2). There appear to be negative or very weak positive correlations between Co and Al_2O_3, TiO_2, P_2O_5, SiO_2, Na_2O, Zn, Pb, Nb, LREE and HREE (Table 1; Fig. 4-1 and Fig. 4-2).

4.2. Mineral compositions of sulfides and sulfoarsenides

Optical microscopy and EPMA analyses show that Co is closely associated with sulfides and sulfoarsenides, occurring as Co-bearing pyrite and Co-rich sulfides/sulfoarsenides. Two kinds of pyrites have been found, i.e. framboidal pyrite and anhedral to euhedral single pyrite. Framboidal pyrite, isolated or clustered, occurs in carbonaceous ferruginous clays (Fig. 5), siderite layers, and bauxitic clay layers (Fig. 6). Anhedral to euhedral pyrite as well as other sulfides including stibnite, chalcopyrite and galena are dispersed in bauxite ores, bauxitic clays, carbonaceous ferruginous clays, and micro-fractures in siderite layers (Long et al., 2017, 2018; Figs. 5, 8 and 9).

Pyrites from the carbonaceous ferruginous clays are subhedral to euhedral microcrystals (~20 to 200 μm in size) with obvious compositional zonation. They are generally clustered to aggregates of various shapes and sizes in a matrix of chamosite, kaolinite, boehmite and diaspore (Fig. 5a and b). EPMA-EDS results show that the rim contains higher content of Co (up to 8.52 wt%) and Ni (up to 6.51 wt%) than the core of the pyrite (Co up to 2.69 wt%; Ni up to 1.18 wt%).

Pyrite framboids from the bauxitic clays and siderite layers appear as spherical aggregates composed of discrete euhedral microcrystals

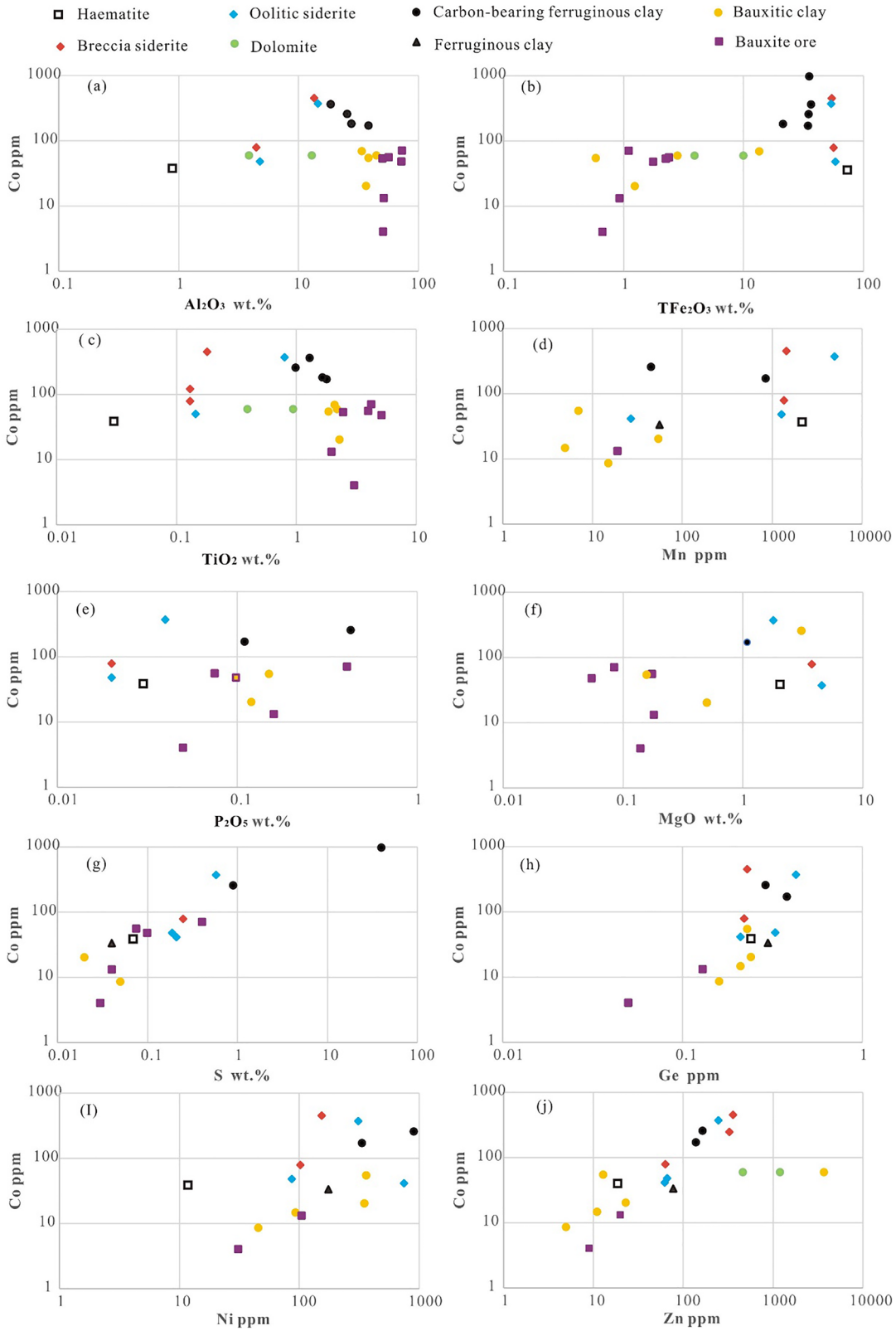

Fig. 4. Binary diagrams of selected elements from whole-rock analyses of samples from the Yunfeng bauxite deposit: (a) Co vs Al_2O_3; (b) Co vs TFe_2O_3; (c) Co vs TiO_2; (d) Co vs Mn; (e) Co vs P_2O_5; (f) Co vs MgO; (g) Co vs S; (h) Co vs Ge; (i) Co vs Ni; (j) Co vs Zn; (k) Co vs Cu; (L) Co vs Pb; (m) Co vs Nb; (n) Co vs HREE; (o) Co vs LREE; (p) Co vs SiO_2; (q) Co vs K_2O and (r) Co vs Na_2O.

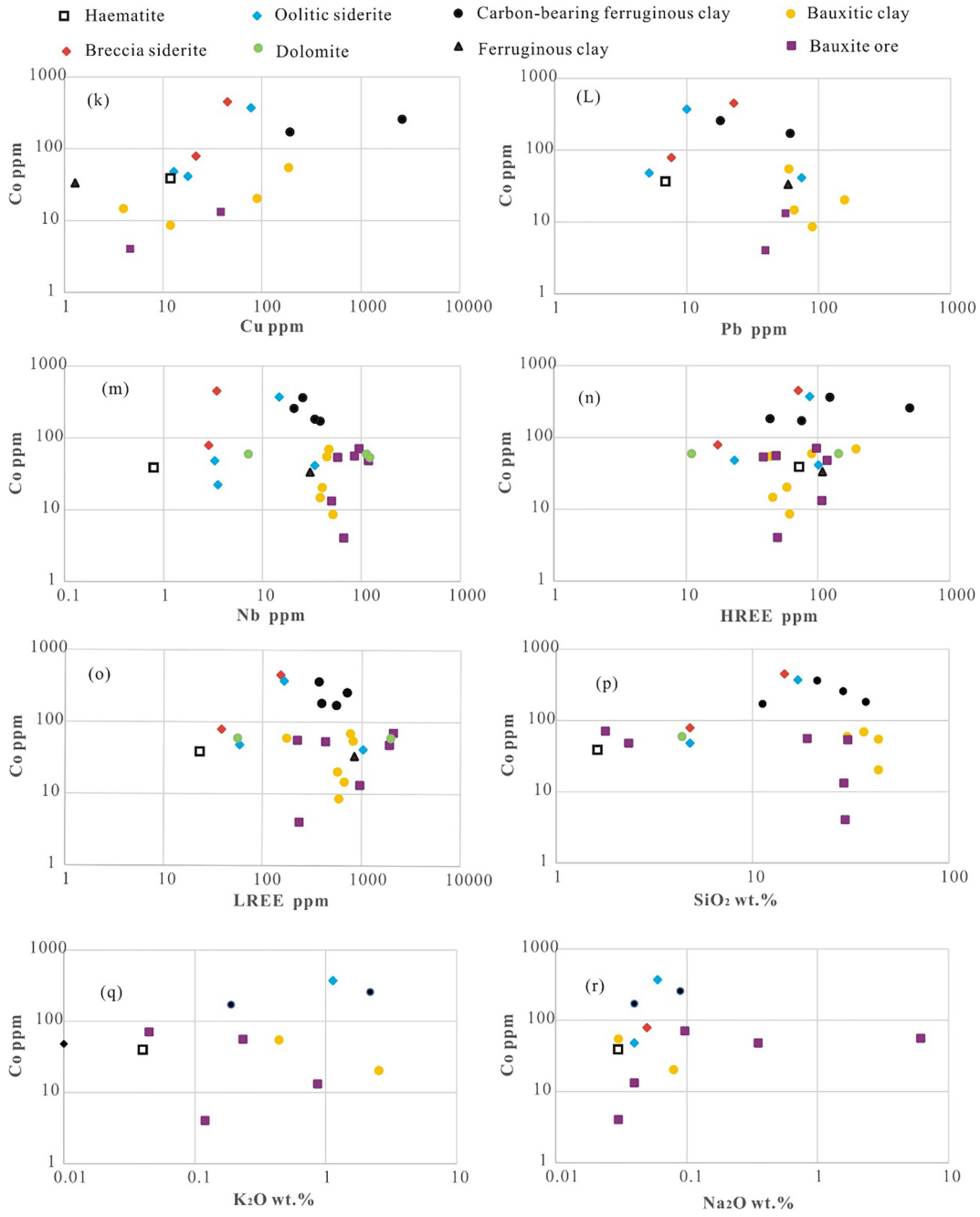

Fig. 4. (*continued*)

(approximately 1 μm in diameter), with variable aggregate sizes from 3 to 12 μm (Figs. 6 and 7). Their Co concentrations are below the detection limit of EPMA-EDS (0.01 wt%). The pyrite framboids in the bauxitic clay layers are distributed in a matrix of kaolinite, diaspore and boehmite, while those from the siderite layers are in a matrix of siderite and carbonaceous matters (Fig. 7). The pyrite framboids have higher concentrations of As in the rims than in the cores (Fig. 7a and b).

Co-rich sulfides/sulfoarsenides are mostly made up of As (34.39–42.25 wt%), Co (18.10–22.45 wt%), S (21.25–27.37 wt%), Fe (4.88–19.58 wt%), Ni (10.46–11.62 wt%) and Sb (0–1.04 wt%). They occur as: (i) euhedral to subhedral grains (~30–50 μm in size) (Fig. 8c and d) in a matrix of diaspore and kaolinite (samples from bauxite ores); (ii) anhedral particles (~50 μm in size) with relict texture (Fig. 5d), zoned grains (~80 μm in size, Fig. 8b), as well as variably-sized (~5 to ~ 60 μm) grains rimmed by uraninite and enclosing an early generation of micron- to nanometer-sized sulfide minerals (Fig. 8a), all occurring in a matrix of kaolinite, boehmite and diaspore (samples from bauxite clays); and (iii) xenomorphic grains (~5–20 μm in size) filling in micro-cracks of the brecciated siderite, closely associated with pyrite and chalcopyrite (Fig. 5h).

Cobalt-bearing pyrites have subhedral to euhedral shapes and variable sizes. They show relict textures and/or compositional zones,

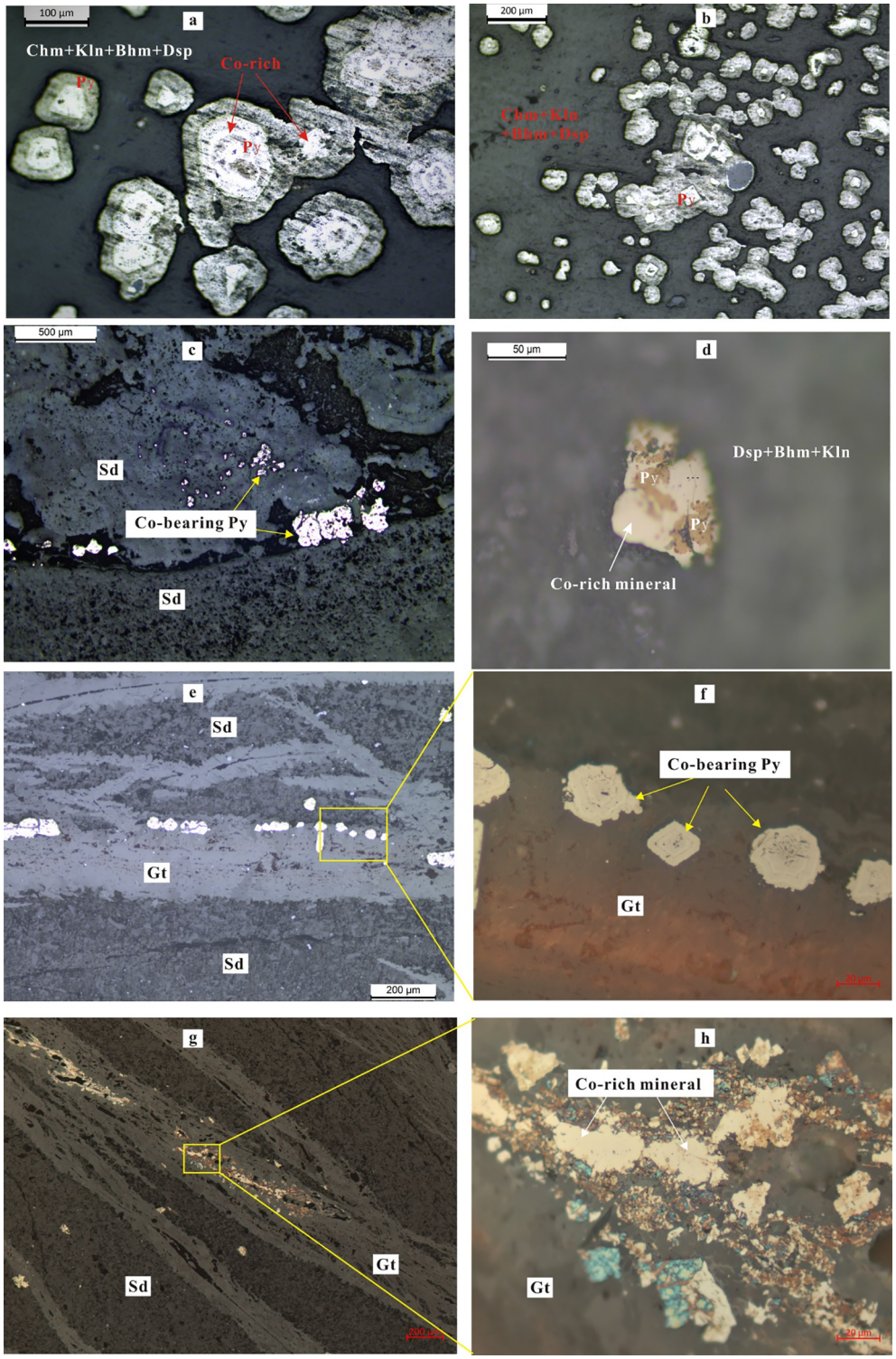

Fig. 5. Photomicrographs of pyrites from the Yunfeng bauxite deposit. (a) Euhedral pyrite with compositional zonation in a matrix of chamosite, kaolinite, boehmite and diaspore (sampled from the bottom carbonaceous ferruginous clay layer); (b) Framboidal pyrites in a matrix of chamosite, kaolinite, boehmite and diaspore (sampled from the upper carbonaceous ferruginous clay layer); (c) Euhedral pyrite in micro-cracks of the brecciated siderite layer; (d) Co-rich sulfide/sulfoarsenide with relict texture in a matrix of diaspore, boehmite and kaolinite (sampled from the lower bauxitic clay layer); (e) and (f) Pyrite with compositional zonation in a micro-crack (sampled from the bottom brecciated siderite layer); (g) and (h) Cobalt-rich sulfide/sulfoarsenide with relict texture in a micro-crack (sampled from the bottom oolitic siderite layer).

and are scattered in carbonaceous ferruginous clays, bauxite ores and bauxitic clays, as well as in micro-cracks of the siderite layers (Fig. 5e, f, g and h). They are composed of Co (2.37–11.78 wt%), As (0.81–18.17 wt%), S (38.65–51.55 wt%), Fe (19.36–32.55 wt%), Ni (11.41–12.72 wt%) and Sb (0–0.63 wt%) (Figs. 5, 8 and 9).

5. Discussion

The findings of extraordinary enrichment of Co, significant correlation between Co and S, as well as occurrence of Co-bearing pyrite and Co-rich sulfides/sulfoarsenides in the Yunfeng bauxite deposit, are of

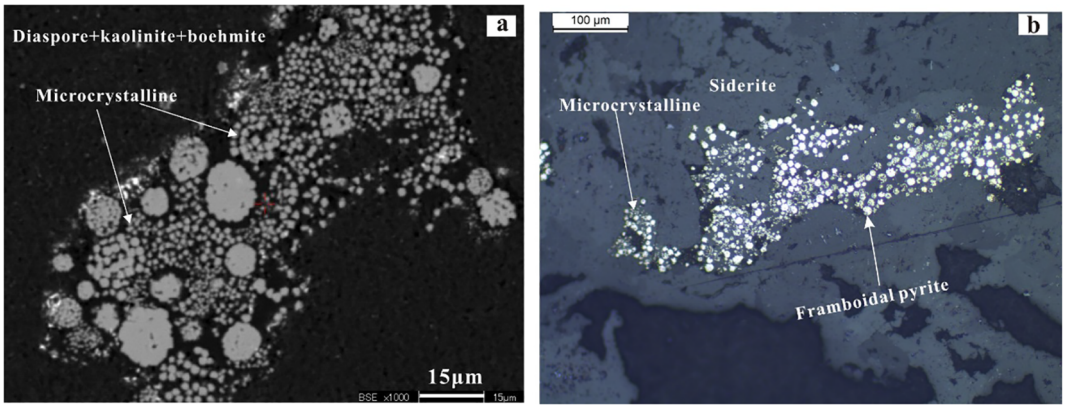

Fig. 6. (a) Backscattered electron (BSE) image of framboidal pyrite from the upper bauxitic clay layer; (b) Photomicrograph of framboidal pyrite from the bottom brecciated siderite layer.

both scientific and economic significance. These are elaborated and discussed as follows.

5.1. Potential scientific significance

For decades, various studies including analytical geochemistry, experimental geochemistry, mineralogy, detrital zircon geochronology and sedimentology, have been tried to clarify the genesis of paleo-karstic bauxite deposits (Mongelli et al., 2014; Wang et al., 2012; Ahmadnejad et al., 2017; Yang et al., 2018). However, it is still a problematic issue due to the diverse sources, paths, and depositional conditions that have been proposed for the formation of these deposits (e.g., Pajović, 2009; Yang et al., 2018). Many previous studies proposed that the paleo-karstic bauxite deposits in central Guizhou Province were derived from weathering of the underlying Loushanguan Group carbonate rocks (Ye et al., 2008; Li et al., 2014; Liu and Liao, 2014; Ling et al., 2017), whereas some studies suggested that they formed from weathering of black shales transported from distance (Long et al., 2017). It is well known that concentration of Co in carbonate rocks is very low (0.1 ppm for pure carbonate rocks, Carr and Turekian, 1961; 1.90 ppm for the Loushanguan Group dolomite, Guizhou, Ji et al., 1999), whereas black shales are commonly rich in Co, e.g. average 19 ppm for black shales worldwide (Carr and Turekian, 1961; Ketris and Yudovich, 2009), 4.3 to 181.4 ppm for Lower Cambrian black shales in Zunyi, Guizhou (Luo et al., 2003; Pi et al., 2013), 13 to 50 ppm for black shales from three major sediment-hosted Au-As provinces (Large et al., 2010), and 19.2 ppm for black shales collected from the upper layer of the Yunfeng deposit in this study (Supplementary Table 1). The finding that Co is significantly enriched in the Yunfeng bauxite deposit provides a strong support for the model in which bauxite formed from weathering of transported black shales (Long et al., 2017).

Under weathering conditions that led to the formation of bauxites, Co(II) and Co(III) can be mobilized from parent rocks into the surficial water (Swanner et al., 2014). However, they are commonly rapidly removed from the solution by sorption and co-precipitation as secondary Fe(III)-oxides/hydroxides and Mn(III, IV)-oxides (e.g., Musić et al., 1979; Takahashi et al., 2007; Koschinsky and Hein, 2003; Stockdale et al., 2010), precipitation as $Co(OH)_3$ (Swanner et al., 2014; Decrée et al., 2015), and complexing with humic and fulvic acids and inorganic colloids (e.g., Mclaren et al., 1986; Collins and Kinsela, 2010). The occurrences of elevated Co in superficial environments (e.g. lateritic Ni-Co deposits) are generally asbolan–lithiophorite group [$(Co, Ni)_{1-y}(MnO_2)_{2-x}(OH)_{2-2y+2x}\cdot nH_2O$], erythrite [$Co_3(AsO_4)_2\cdot 8H_2O$], heterogenite [CoO(OH)], and cobaltiferous oxides/hydroxides (goethite and limonite) (Swanner et al., 2014; Gigler and Kinnaird, 2017).

In the Yunfeng bauxite deposit, the rocks with elevated cobalt concentrations are relatively rich in Fe oxides/hydroxides, as reflected by the moderate positive correlation between Co and TFe_2O_3 (Fig. 4-1b) as well as Mn (Fig. 4d). This may appear to be consistent with previous studies of Co enrichment in lateritic Ni-Co deposits formed from weathering of ultramafic rocks (Decrée et al., 2015; Muchez and Corbella, 2012; Yongue-Fouateu et al., 2006; Pazik et al., 2016; Ugwu and Sherman, 2017). However, the fact that Co occurs principally as Co-bearing pyrites and Co-rich sulfides/sulfoarsenides in the Yunfeng bauxite deposit, rather than as cobaltiferous oxides/hydroxides as in lateritic Ni-Co deposits (Swanner et al., 2014; Gigler and Kinnaird, 2017), suggests that the Co enrichment mechanism in the bauxite deposits is different from those associated with the lateritic Ni-Co deposits.

Co(III) is not thermodynamically stable and decomposes under Eh-pH conditions common for most natural waters (Krupka and Serne, 2002), only possibly precipitated as $Co(OH)_3$ at very high Eh–pH conditions (Swanner et al., 2014; Decrée et al., 2015). In contrast, Co(II) is a relatively stable valence state and exists dominantly as simple ion Co^{2+} (pH < 9.5) and hydrolytic species Co(OH)2° (aq; 9.5 < pH < 13.5) in oxidizing and moderately reducing conditions, while in very reducing conditions plus presence of dissolved sulfides, it exhibits as Co^{2+} bisulfide species (Krupka and Serne, 2002). Cobalt generally exists as solid solution with other transition metal elements, such as Mn^{4+}, Fe^{2+}, Fe^{3+} and Ni^{2+} in sulfide/sulfoarsenide minerals, due to the similarity of ionic radii between Co^{2+}/Co^{3+} and these elements (Manceau et al., 1997; Krupka and Serne, 2002; Swanner et al., 2014). The concentration of Co in sulfides/sulfoarsenides is largely dependent on the physical and chemical conditions of the fluid system from which they were precipitated (Craig et al., 1998; Velásquez et al., 2014; George et al., 2016). The dominant occurrence of Co in sulfides/sulfoarsenides in the Yunfeng bauxite deposit reflects a relatively reducing environment, which is different those associated with the lateritic Ni-Co deposits. On the other hand, the development of compositional zoning of Co-bearing/rich pyrites (Fig. 5a, b and f; Fig. 8a and b, and Fig. 9) reflects a dynamic environment with varying redox conditions. Overall, the physicochemical conditions of the Yunfeng bauxite deposit possibly evolved from a relatively oxidizing environment during weathering

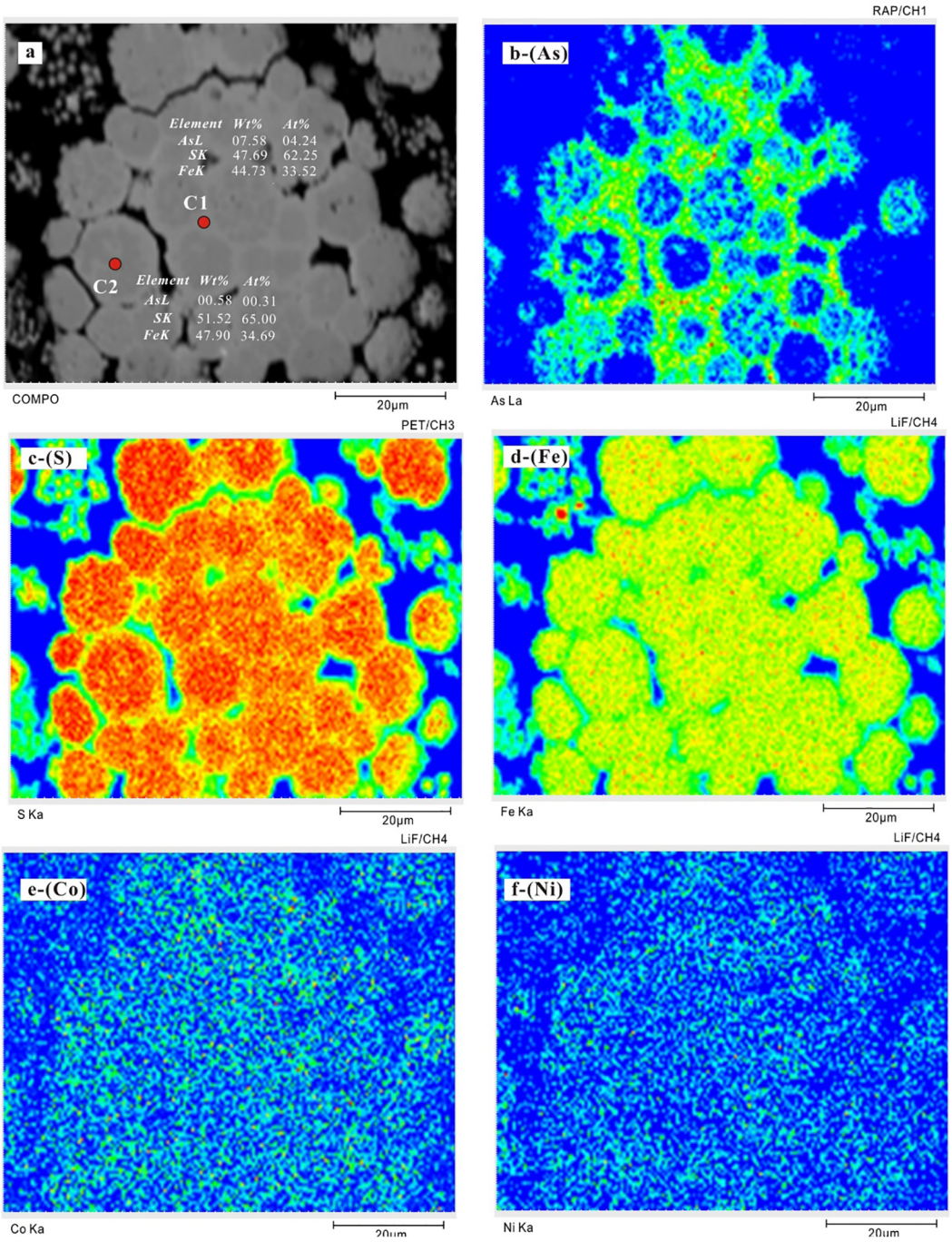

Fig. 7. (a) Backscattered electron image (BSE) and (b–f) EPMA mappings of framboidal pyrite in a matrix of kaolinite, boehmite and diaspore (sampled from the lower bauxitic clay layer).

period to increasingly reducing conditions during diagenesis (Long et al., 2018).

5.2. Potential economic significance

Bauxite resources are abundant in China (primarily in paleo-karstic deposits), ranking as the fifth major bauxite province in the world, next to Guinea, Australia, Brazil, and Jamaica (Wang et al., 2010; Huang et al., 2014; Ling et al., 2015). Guizhou Province hosts some of the largest economic bauxite deposits in China. The total proven and potential bauxite resource of Guizhou is up to 1 Bt (Long et al., 2018). The results of this study suggest that the Co resource in the bauxite ores may be of potential economic value. Because Co occurs dominantly as Co-rich sulfides/sulfoarsenides and Co-bearing pyrite, it is relatively easy

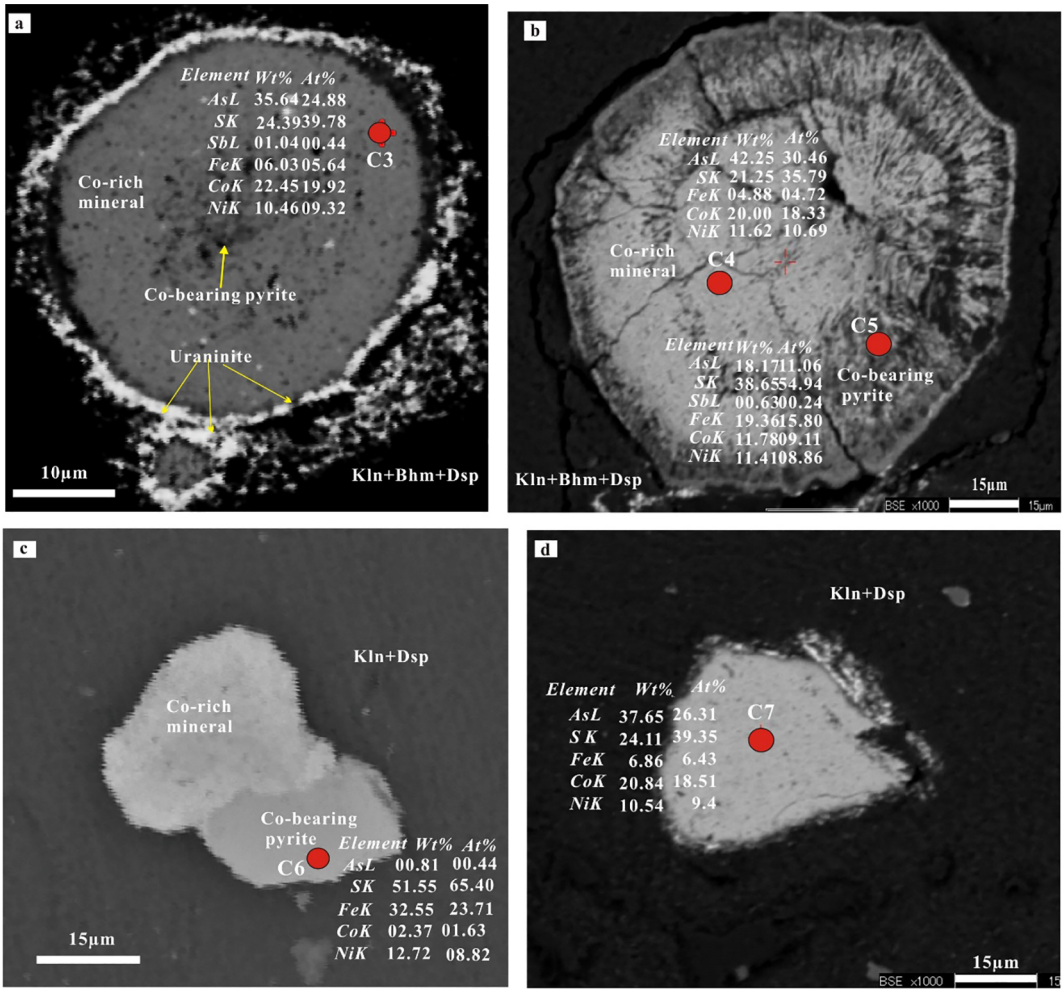

Fig. 8. (a) and (b) Backscattered electron (BSE) images of Co-rich sulfide/arsenide and Co-bearing pyrite (bauxitic clays); (c) BSE image of Co-rich sulfide/arsenide closely associated with Co-bearing pyrite (bauxite ore); (d) BSE image of Co-rich sulfide/arsenide (bauxite ore). Klm-kaolinite; Dsp-diaspore; Bhm-boehmite; Py-pyrite.

to be recovered as by-product of bauxite ores; the cut-off grade of Co for sulfides or arsenides is only 200 ppm and the minimum grade of Co for economic exploitation from this kind of ore is only 300 ppm (Sun, 2000). The average concentrations of Co in the siderite layers (212.8 ppm) and carbonaceous ferruginous clay layers (383 ppm) are higher than the cut-off grade and minimum economic grade, respectively. Considering that the Co-enriched layers in the Yunfeng bauxite deposit may reach 0.5–3 m in thickness, and the same layers may be present in similar bauxite deposits that are extensively distributed in Guizhou (Fig. 1a), significantly amounts of Co may be potentially recovered from production of bauxites. Furthermore, since Co enrichment has also been reported in other paleo-karstic bauxite deposits elsewhere in the world, the results documented in this paper may invoke similar and new studies to further evaluate the economic value of Co resources in these deposits.

6. Conclusions

This study examines the concentration, occurrence, and distribution of Co in the Yunfeng paleo-karstic bauxite deposit, through whole-rock geochemistry and mineralogy of rocks from various layers of the deposit. The following conclusions are reached based on these studies.

(1) Several layers of rocks in the Yunfeng bauxite deposit are characterized by high contents of Co, especially for the carbonaceous ferruginous clay layers (167–962 ppm) and the siderite layers (47–439 ppm). These Co-enriched layers may reach 0.5–3 m in thickness.
(2) The strong positive correlation between Co and S from the whole-rock geochemical data, coupled with EPMA and EDS analyses, indicates that Co occurs chiefly as Co-rich sulfides/sulfoarsenides and Co-bearing pyrite. These sulfides and sulfoarsenides are scattered in a matrix of diaspore, kaolinite, and/or boehmite (layers of bauxite ores, bauxitic clays and carbonaceous ferruginous clays), or in a matrix of Fe-, Al- and Mn-oxides/hydroxides and carbonaceous materials (siderite layers).
(3) The significant thicknesses of the Co-enriched layers in the Yunfeng bauxite deposit and potentially in other bauxite deposits in Guizhou Province, together with the relatively easy recovery of Co from sulfides and sulfoarsenides, make the paleo-karstic bauxite deposits a potential Co resource.

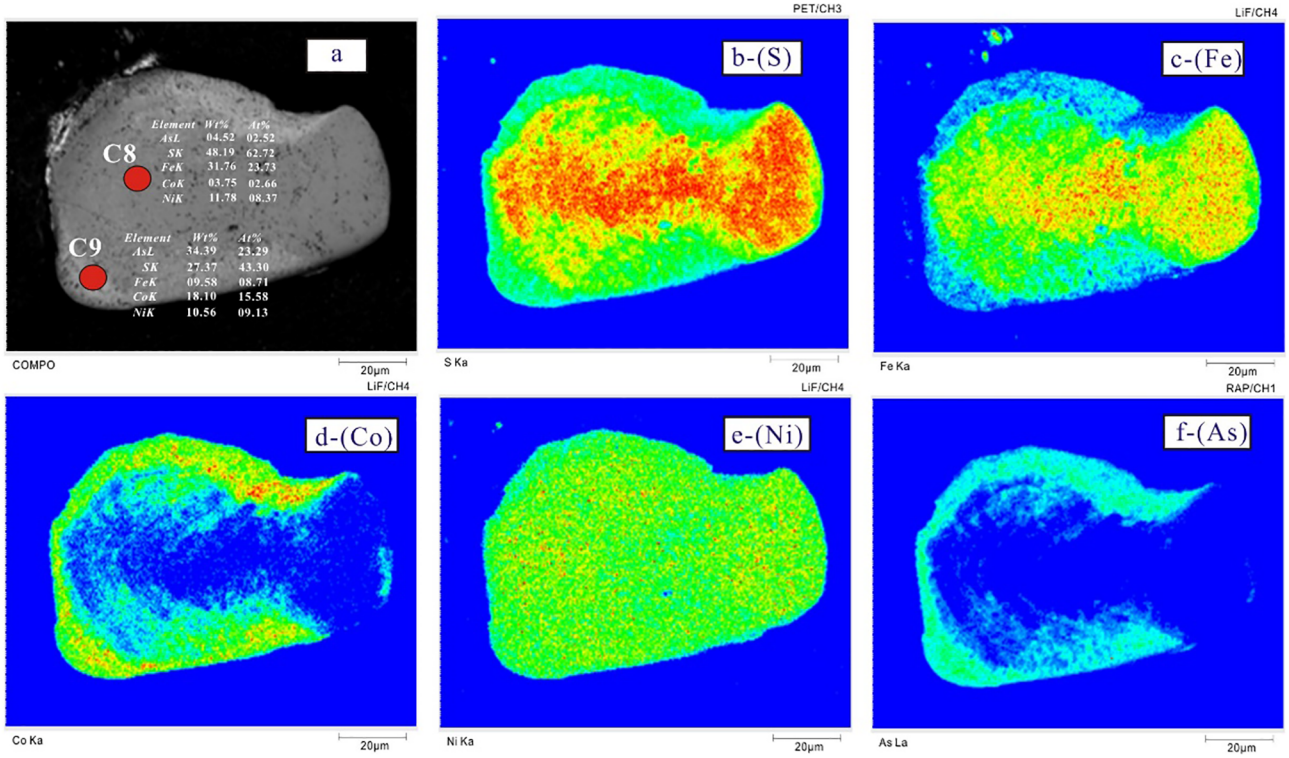

Fig. 9. (a) Backscattered electron (BSE) image and (b–f) EPMA mappings of Co-rich and Co-bearing sulfide/arsenide (bauxitic clay). Co and As are enriched in the rim, and S and Fe are enriched in the core, whereas Ni does not show any systematic variation between the rim and the core.

Declaration of Competing Interest

The authors declare that they have no known competing financial interests or personal relationships that could have appeared to influence the work reported in this paper.

Acknowledgments

This work was jointly supported by the Key Laboratory of Metallogenic Prediction of Nonferrous Metals and Geological Environment Monitoring, Ministry of Education, Central South University (No. 2019YSJS04, No. 2018YSJS01), National Program on Key Basic Research Project (973 Program: 2014CB440901), and the National Natural Science Foundation of China (Grant No. 41673056). We would like to thank two anonymous reviewers and Dr. Franco Pirajno for constructive comments that helped improve this paper.

Appendix A. Supplementary data

Supplementary data to this article can be found online at https://doi.org/10.1016/j.oregeorev.2019.103308.

References

Ahmadnejad, F., Zamanian, H., Taghipour, B., Zarasvandi, A., Buccione, R., Ellahi, S.S., 2017. Mineralogical and geochemical evolution of the Bidgol bauxite deposit, Zagros Mountain Belt, Iran: Implications for ore genesis, rare earth elements fractionation and parental affinity. Ore Geol. Rev. 86, 755–783.

Bárdossy, G., Aleva, G., 1990. Lateritic Bauxites. Elsevier Scientific Publication, Amsterdam, pp. 1–624.

Bogatyrev, B., Zhukou, V., Tsekhovsky, Y.G., 2009. Formation conditions and regularities of the distribution of large and superlasrge bauxite deposits. Lithol. Min. Resour. 44, 135–151.

Bonnetti, C., Cuney, M., Malartre, F., Michels, R., Liu, X., Peng, Y., 2015. The Nuheting deposit, Erlian Basin, NE China, Synsedimentary to diagenetic uranium mineralization. Ore Geol. Rev. 69, 118–139.

Cailteux, J., Kampunzu, A., Lerouge, C., Kaputo, A.K., Milesi, J., 2005. Genesis of sediment-hosted stratiform copper–cobalt deposits, Central African Copperbelt. J. Afr. Earth. Sci. 42, 134–158.

Carr, M.H., Turekian, K.K., 1961. The geochemistry of cobalt. Geochim. Cosmochim. Act. 23, 9–60.

Collins, R., Kinsela, A., 2010. The aqueous phase speciation and chemistry of cobalt in terrestrial environments. Chemosphere 79, 763–771.

Craig, J.R., Vokes, F.M., Solberg, T.N., 1998. Pyrite: physical and chemical textures. Miner. Deposita 34, 82–101.

Decrée, S., Pourret, O., Baele, J.M., 2015. Rare earth element fractionation in heterogenite (CoOOH): implication for cobalt oxidized ore in the Copperbelt (Democratic Republic of Congo). J. Geochem. Explor. 159, 290–301.

Desouky, H., Muchez, P., Boyce, A., Schneider, J., Cailteux, J., Dewaele, S., Quadt, A., 2010. Genesis of sediment-hosted stratiform copper–cobalt mineralization at Luiswishi and Kamoto, Katanga Copperbelt (Democratic Republic of Congo). Miner. Deposita 45, 735–763.

Fay, I., Barton, M.D., 2012. Alteration and ore distribution in the Proterozoic Mines Series, Tenke-Fungurume Cu–Co district, Democratic Republic of Congo. Miner. Deposita 47, 501–519.

George, L.L., Cook, N.J., Ciobanu, C.L., 2016. Partitioning of trace elements in co-crystallized sphalerite–galena–chalcopyrite hydrothermal ores. Ore Geol. Rev. 77, 97–116.

Gervill, F., Sancnez-anguita, A., Acevedo, R.D., Hach-ali, P.F., Paniagu, A., 1997. Platinum-group element sulpharsenides and Pd bismuthotellurides in the metamorphosed Ni-Cu deposit at Las Aguilas (Province of San Luis, Argentina). Mineral. Mag. 61, 861–877.

Gigler, G.M., Kinnaird, J.A., 2017. Element mobility in the weathering environment and surface vectors to mineralization – A case study from the Mashitu South Cu-Co deposit, Katanga, Democratic Republic of Congo. J. Geochem. Explor. 183, 127–137.

Gregory, D.D., Large, R.R., Halpin, A.J., Baturina, E.L., 2015. Trace Element Content of Sedimentary Pyrite in Black Shales. Econ. Geol. 110, 1389–1410.

Grorud, H.F., 1997. Textural and compositional characteristics of cobalt ores from the Skuterud Mines of Modum, Norway. Norw. J. Geol. 77, 31–38.

Guizhou Bureau of Geology and Mineral Resources, 1987. Geological Features of Guizhou Province. Geological Publishing House, Beijing, pp. 1–360 (in Chinese).

Huang, Z.L., Jin, Z.G., Xiang, X.L., Gu, J., Wu, G.H., Chen, X.L., Su, Z.L., Zho, Y.Y., Zuo, L., 2014. Mectallogenic Theory and prediction of bauxite deposits in the Wuchunan-

Zheng'an-Daozhen area, Northern Guizhou province, China. Science Press, pp. 89–99 (in Chinese).
Hughes, H., McDonald, I., Faithfull, J., Upton, B., Loocke, M., 2016. Cobalt and precious metals in sulfides of peridotite xenoliths and inferences concerning their distribution according to geodynamic environment – a case study from the Scottish lithospheric mantle. Lithos 240–243, 202–227.
Ingham, E.S., Cook, N., Cliff, J., Ciobanu, C.L., Huddleston, A., 2014. A combined chemical, isotopic and microstructural study of pyrite from roll-front uranium deposits, Lake Eyre Basin, South Australia. Geochim. Cosmochim. Acta 125, 440–465.
Ji, H.B., Ouyang, Z.Y., Wang, S.J., Zhou, D.Q., 1999. Element geochemical characteristics of the dolomite weathering profile and its significance to the upper continental crust average chemical composition, as Xin Pu profile, North Guizhou for an example. Sci. China (D) 29, 504–513 (in Chinese with English abstract).
Ketris, M.P., Yudovich, Y.E., 2009. Estimations of Clarkes for Carbonaceous biolithes: World averages for trace element contents in black shales and coals. Int. J. Coal. Geol. 78, 135–148.
Kissin, S.A., 1992. Five-element (Ni-Co-As-Ag-Bi) veins. Geosci. Can. 19, 113–124.
Koschinsky, A., Hein, J.R., 2003. Uptake of elements from sea water by ferromanganese crusts: solid-phase association sand sea water speciation. Mar. Geol. 198, 331–351.
Krupka, K.M., Serne, R. J., 2002. Geochemical Factors Affecting the Behavior of Antimony, Cobalt, Europium, Technetium, and Uranium in Vadose Sediments, Prepared for CH2M HILL Hanford Group, Inc., and the U.S. Department of Energy under Contract DE-AC06-76RL01830, Pacific Northwest National Laboratory Richland, Washington, pp.1-95.
Large, D.J., Sawlowicz, Z., Spatt, J., 1999. A cobaltite-framboidal pyrite association from the Kupferschiefer: possible implications for trace element behavior during the earliest stages of diagenesis. Mineral. Mag. 63, 353–361.
Large, R.R., Bull, S., Maslennikov, V., 2010. A carbonaceous sedimentary source-rock model for Carlin-type and orogenic gold deposits. Econ. Geol. 106, 331–358.
Lefebure, D.V., 1996. Five-element Veins Ag-Ni-Co-As+/-(Bi,U). In: Selected British Columbia Mineral Deposit Profiles, Volume 2 – Metallic Deposits, Lefebure, D.V. and Höy, T, Editors, British Columbia Ministry of Employment and Investment, Open File 1996-13, 89-92.
Li, Z., Liu, J., Zhang, C., 2008. Ore-forming material sources of the Baiyangping Cu-Co-Ag polymetallic deposit in the Lanping Basin, western Yunnan Province. Chin. J. Geochem. 27, 217–224 (in Chinese).
Li, Y.T., Xiao, J.F., Fu, S.H., Zhao, Z.J., 2014. The comparison study on metallogenic characteristics of the main bauxite-deposit-clustered areas in Guizhou province. Contributions to Geology and Mineral Resources Research 4, 489–494 (in Chinese with English abstract).
Ling, K.Y., Zhu, X.Q., Tang, H.S., Wang, Z.G., Yan, H.W., Han, T., Chen, W.Y., 2015. Mineralogical characteristics of the karstic bauxite deposits in the Xiuwen ore belt, Central Guizhou Province, Southwest China. Ore Geol. Rev. 65, 86–96.
Ling, K.Y., Zhu, X.Q., Tang, H.S., Li, S.X., 2017. Importance of hydrogeological conditions during formation of the karstic bauxite deposits, Central Guizhou Province, Southwest China: A case study at Lindai deposit. Ore Geol. Rev. 82, 198–216.
Liu, P., Liao, Y.H., 2014. Regional metallogenic model and prospecting criteria of sedimentary bauxite deposits in Central Guizhou—Southern Chongqing region. Geol. China 41, 2063–2082 (in Chinese with English abstract).
Long, Y., Chi, G., Liu, J., Jin, Z., Dai, T., 2017. Trace and rare earth elements constraints on the sources of the Yunfeng paleo-karstic bauxite deposit in the Xiuwen-Qingzhen area, Guizhou. China. Ore Geol. Rev. 91, 404–418.
Long, Y., Chi, G., Liu, J., Zhang, D., Song, H., 2018. Uranium enrichment in a paleo-karstic bauxite deposit, Yunfeng, SW China: mineralogy, geochemistry, transport - deposition mechanisms and significance for uranium exploration. J. Geochem. Explor. 190, 424–435.
Luo, T., Zhang, H., Li, X., Zhu, D., 2003. Mineralization characteristics of the multi-element-rich strata in the Niutitang Formation black shale series, Zunyi, Guizhou, China. Acta Mineral. Sinica 23, 296–302 (in Chinese with English abstract).
Manceau, A., Drits, V.A., Silvester, E., Bartoli, C., Lanson, B., 1997. Structural mechanism of Co^{2+} oxidation by the phyllomanganate buserite. Am. Mineral. 82, 1150–1175.
Mclaren, R.G., Lawson, D.M., Swift, R.S., 1986. Sorption and desorption of cobalt by soils and soil components. Eur. J. Soil. Sci. 37, 413–426.
Mongelli, G., Boni, M., Buccione, R., Sinisi, R., 2014. Geochemistry of the Apulian karst bauxites (southern Italy): chemical fractionation and parental affinities. Ore Geol. Rev. 63, 9–21.
Mongelli, G., Boni, M., Oggiano, G., Mameli, P., Sinisi, R., Buccione, R., Mondillo, N., 2017. Critical metals distribution in Tethyan karst bauxite, the cretaceous Italian ores. Ore Geol. Rev. 86, 526–536.
Muchez, P., Corbella, M., 2012. Factors controlling the precipitation of copper and cobalt minerals in sediment-hosted ore deposits: Advances and restrictions. J. Geochem. Explor. 118, 38–46.
Musić, S., Gessner, M., Wolf, R., 1979. Sorption of small amounts of cobalt(II) on iron(III) oxide. Microchim. Acta 71, 105–112.
Naldrett, A.J., Singh, J., Krstic, S., Li, C., 2000. The mineralogy of the Voisey's Bay Ni–Cu–Co deposit, northern Labrador, Canada: influence of oxidation state on textures and mineral compositions. Econ. Geol. 95, 889–900.
Naumov, G.B., Golubev, V.N., Vlasov, B.P., Mironov, O.F., 2017. The Schlema-Alberoda five-element uranium deposit, Germany: an example of self-organizing hydrothermal system. Geol. Ore. Deposit. 59, 1–13.
Nimis, P., Costa, D.L., Guastoni, A., 2014. Cobaltite-rich mineralization in the iron skarn deposit of Traversella (Western Alps, Italy). Mineral. Mag. 78, 11–27.
Pajović, M., 2009. Genesis and genetic types of karst bauxites. Iran. J. Earth Sci. 1, 44–56.
Pazik, P.M., Chmielewski, T., Glass, H.J., Kowalczuk, P.B., 2016. World production and possible recovery of cobalt from the Kupferschiefer stratiform copper core. E3S Web of Conferences 8, 1-9.
Pi, D.H., Liu, C.Q., Shields-Zhou, G.A., Jiang, S.Y., 2013. Trace and rare earth element geochemistry of black shale and kerogen in the early Cambrian Niutitang Formation in Guizhou province, South China: Constraints for redox environments and origin of metal enrichments. Precamb. Res. 225, 218–229.
Qi, L., Hu, J., Gregoire, D.C., 2000. Determination of trace elements in granites by inductively coupled plasma mass spectrometry. Talanta 51, 507–513.
Radusinović, S., Jelenković, R., Pačevski, A., Simić, V., Božović, D., Holclajtner-Antunović, I., Životić, D., 2017. Content and mode of occurrences of rare earth elements in the Zagrad karstic bauxite deposit (Nikšić area, Montenegro). Ore Geol. Rev. 80, 406–428.
Saintilan, N.J., Creaser, R.A., Bookstrom, A.A., 2017. Re-Os systematics and geochemistry of cobaltite (CoAsS) in the cobalt belt, Belt-Purcell Basin, USA: Evidence for middle Mesoproterozoic sediment-hosted Co-Cu sulfide mineralization with Grenvillian and Cretaceous remobilization. Ore Geol. Rev. 86, 509–525.
Sibbald, T., 1985. Geology and genesis of the Athabasca Basin uranium deposits. In: Summary of Investigations 1985, Saskatchewan Geological Survey, Saskatchewan Energy and Mines, Miscellaneous Report, 85-4.
Stockdale, A., Davison, W., Zhang, H., Hamilton-Taylor, J., 2010. The association of cobalt with Fe-, Mn- (oxyhydr) oxides in marine sediment. Aquat. Geochem. 16, 575–585.
Sun, C., and compilation committee (36 members), 2000. Comprehensive utilization of mineral resources. Science Press, 835 p (in Chinese).
Swanner, E.D., Planavsky, N.J., Lalonde, S.V., Robbins, L.J., Bekker, A., Rouxel, O.J., Saito, M.A., Kappler, A., Mojzsis, S.J., Konhauser, K.O., 2014. Cobalt and marine redox evolution. Earth. Planet. Sc. Lett. 390, 253–263.
Takahashi, Y., Manceau, A., Geoffroy, N., Marcus, M.A., Usui, A., 2007. Chemical and structural control of the partitioning of Co, Ce, and Pb in marine ferromanganese oxides. Geochim. Cosmochim. Acta 71, 984–1008.
Taylor, S.R., McLennan, S.M., 1985. The continental crust: its composition and evolution. Blackwell, Oxford, pp. 1–312.
Ugwu, I.M., Sherman, D.M., 2017. Irreversibility of sorption of cobalt to goethite (α-FeOOH) and disparities in dissolution of aged synthetic Co-goethite. Chem. Geol. 467, 168–176.
Velásquez, G., Béziat, D., Salvi, S., Siebenaller, L., Borisova, A.Y., Pokrovski, G.S., De Parseval, P., 2014. Formation and deformation of pyrite and implications for gold mineralization in the El Callao District, Venezuela. Econ. Geol. 109, 457–486.
Wagner, T., Lorenz, J., 2002. Mineralogy of complex Co-Ni-Bi vein mineralization, Bieber deposit, Spessart, Germany. Mineral. Mag. 66, 385–407.
Wang, Q.F., Deng, J., Liu, X.F., Zhang, Q.Z., Sun, S.L., Jiang, C.Z., Zhou, F., 2010. Discovery of the REE minerals and its geological significance in the Quyang bauxite deposit, West Guangxi, China. J. Asian. Earth. Sci. 39, 701–712.
Wang, Q.F., Liu, X.F., Yan, C.H., Cai, S.H., Li, Z.M., Wang, Y.R., Zhao, J.M., Li, G.J., 2012. Mineralogical and geochemical studies of boron-rich bauxite ore deposits in the Songqi region, SW Henan, China. Ore Geol. Rev. 48, 258–270.
Yang, S., Wang, Q., Zhang, Q., Chen, J., Huang, Y., 2018. Terrestrial deposition processes of Quaternary gibbsite nodules in the Yongjiang Basin, southeastern margin of Tibet, and implication for the genesis of ancient karst bauxite. Sediment. Geol. 373, 292–306.
Ye, L., Pan, Z., Cheng, Z., 2008. The regularities of distribution of associated elements in Xiaoshanba bauxite deposit, Guizhou. Acta Mineral. Sinica 28, 105–111 (in Chinese with English abstract).
Yongue-Fouateu, R., Ghogomu, R.T., Penaye, J., Ekodeck, G.E., Stendal, H., Colin, F., 2006. Nickel and cobalt distribution in the laterites of the Lomié region, south-east Cameroon. J. Afr. Earth. Sci. 45, 33–47.
Zhang, Z.W., Zhou, L.J., Li, Y.J., Wu, C.Q., Zheng, C.F., 2013. The "coal-bauxite-iron" structure in the ore-bearing rock series as a prospecting indicator for southeastern Guizhou bauxite mines. Ore Geol. Rev. 53, 145–158.
Zou, S., Zou, F., Ning, J., Deng, T., Yu, D., Xu, D., Wang, Z., 2018. A stand-alone Co mineral deposit in northeastern Hunan Province, South China: Its timing, origin of ore fluids and metal Co, and geodynamic setting. Ore Geol. Rev. 92, 42–60.